# CHAPTER 2
# ELECTROSPINNING OF LINEAR HOMOPOLYMERS OF POLY(METHYL METHACRYLATE):EXPLORING RELATIONSHIPS BETWEEN FIBER FORMATION, VISCOSITY, MOLECULAR WEIGHT AND CONCENTRATION IN A GOOD SOLVENT[†]

## 2.1 Chapter Summary

A series of seven linear homopolymers of poly(methylmethacrylate) ranging from 12,470 – 365,700 g/mol $M_w$, were utilized to further explore scaling relationships between viscosity, and concentration in a good solvent at 25 $^oC$ and to investigate the impact of these relationships on fiber formation during electrospinning. For each of the polymers investigated, chain dimensions (hydrodynamic radius and radius of gyration) were measured by dynamic light scattering to determine the critical chain overlap concentration, c*. The experimentally determined c*, was found to be in good agreement with the theoretically determined value that was calculated by the criteria $\mathbf{c^*} \sim 1/[\eta]$, where the intrinsic viscosity was estimated from the Mark-Houwink parameters, *K* and *a* (at 25 $^oC$ in dimethyl formamide) obtained from the literature. The plot of the zero shear viscosity versus c/c* distinctly separated into different solution regimes, viz., dilute (c/c*<1), semidilute unentangled (1<c/c*<3) and semidilute entangled (c/c*>3). The crossover between semidilute unentangled and semidilute entangled regimes in the present investigation occurred at c/c*~3, which therefore marked the onset of the critical chain entanglement concentration, $c_e$, according to the procedure utilized by Colby and coworkers *(J. Phys. Chem. B. 2002, 106 (27), 6887)*. Electrospinning of all solutions was carried out at identical conditions to ascertain the effects of solution concentration, molecular weight, molecular weight distribution and viscosity on fiber formation and morphological features of the electrospun material. Only polymer droplets were observed to form from electrospinning of solutions in the dilute concentration regime due to insufficient chain overlap. As the concentration was increased, droplets and beaded fibers were observed in the semidilute unentangled regime; and beaded as well as uniform fibers were observed in the semidilute entangled regime. Uniform fiber formation was

[†] P. Gupta, C. Elkins, T. Long, G. Wilkes, manuscript submitted to *Polymer*

observed at c/c*~6 for all the narrow MWD polymers ($M_w$ of 12,470-205,800 g/mol) but for the relatively broad MWD polymers ($M_w$ of 34,070 and 95,800 g/mol), uniform fibers were not formed until higher concentrations, c/c*~10, were utilized. Dependence of fiber diameter on concentration and viscosity was also determined, viz., *fiber dia ~ (c/c*)*$^{3.1}$ and *fiber dia* ~ $\eta_o^{0.71}$ respectively. These scaling relationships were in general agreement with that observed by Mckee et al *(Macromolecules 2004, 37(5), 1760)*.

**Keywords:** Electrospinning, concentration, viscosity, chain overlap.

## 2.2 Introduction

Electrospinning is a unique process to produce submicron polymeric fibers in the average diameter range of 100 nm-5 μm.[1-4] Fibers produced by this approach are at least one or two orders of magnitude smaller in diameter than those produced by conventional fiber production methods like melt or solution spinning.[5] In a typical electrospinning process (Figure 2.1), described extensively in the literature,[6-10] a jet is ejected from the surface of a charged polymer solution when the applied electric field strength (and consequently the electrostatic repulsion on the surface of the fluid) overcomes the surface tension. The ejected jet travels rapidly to the collector target located at some distance from the charged polymer solution under the influence of the electric field and becomes collected in the form of a solid polymer filament as the jet dries. During its flight to the target, the jet undergoes a series of electrically driven bending instabilities[11-15] that gives rise to a series of looping and spiraling motions. In order to minimize the instability caused by the repulsive electrostatic charges, the jet elongates to undergo large amounts of plastic stretching that consequently leads to a significant reduction in its diameter. However, the degree of molecular orientation in a fiber spun from a solution of an amorphous polymer is not generally high. This is due to the high molecular mobility in fibers containing solvents[16] (chain relaxation is often faster than the time it takes for the solvent to evaporate completely from the fiber). The extremely small diameter electrospun fibers possess a high aspect ratio that promotes a larger specific surface. As a result, they have potential applications ranging from optical[17, 18] and chemo-sensor materials,[19] nanocomposite materials,[20] nanofibers with specific surface chemistry[21] to tissue scaffolds, wound dressings, drug delivery systems,[9, 10, 22-29] filtration and protective clothing.[30]

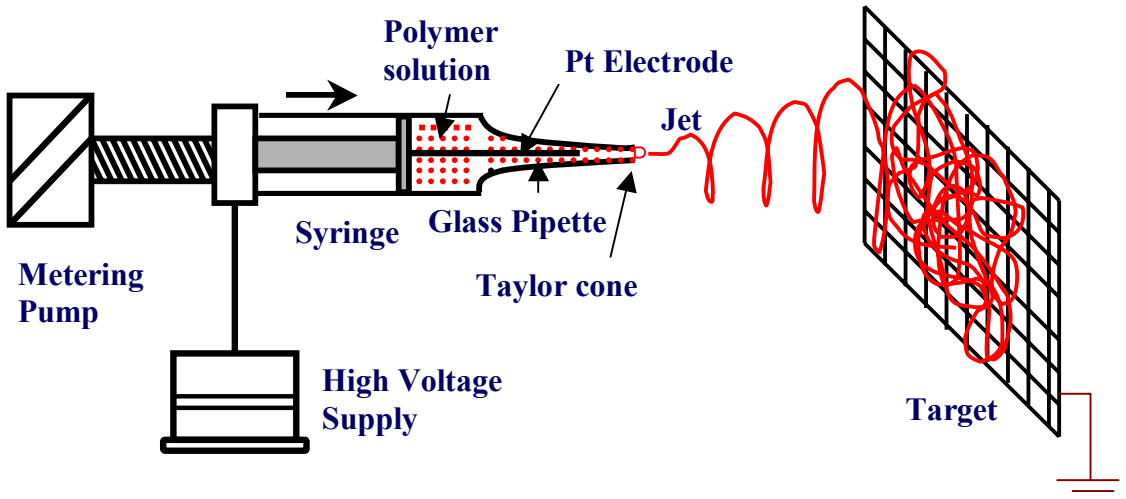


**Figure 2.1** Schematic of the electrospinning apparatus utilized to electrospin PMMA solutions

Current research efforts have focused in understanding the formation, shape, texture and morphology of electrospun fibers. In fact, the principal parameters that affect fiber diameter are as follows:[1, 2, 31-34] *system parameters* – viscosity, net charge density (conductivity), surface tension of the polymer fluid, molecular weight, molecular weight distribution and topology (branched, linear etc.) of the polymer; *process parameters* - electric field strength (electric potential and tip-target separation distance), flow rate of the polymer solution, concentration, ambient parameters (temperature, humidity and air velocity in the electrospinning chamber), internal diameter of the nozzle/capillary, and motion of the target substrate. In the past, the effect of various parameters, particularly viscosity and surface tension, on fiber diameter has been investigated.[2] It has also been observed that increasing the concentration (and consequently viscosity) while lowering the surface tension favors the formation of bead-free and uniform fibers.[34-36] A direct correlation has been observed between *uniform* fiber diameter and solution viscosity,[33, 34] however, more detailed investigations on the dependence of fiber formation and fiber morphology on molecular weight (MW), molecular weight distribution (MWD), topology and solution rheology need to be done. Work from the authors' laboratories was recently

conducted by McKee et al[33], that focused on the effect of solution rheological behavior on fiber morphology of linear and branched copolymers (11,700-106,00 g/mol $M_w$) of poly(ethylene terephthalate-co-ethylene isopthalate) (PET-co-PEI) that were electrospun from a good solvent combination of 70/30 w/w mixture of chloroform and *N,N*-dimethyl formamide ($CHCl_3$/DMF). In that study, investigation of the dependence of electrospun fiber diameter on concentration in the semidilute entangled and concentrated regime was made, in addition to investigating correlations between viscosity and concentration in different concentration regimes. A systematic approach to investigate electrospun *fiber formation* in different concentration regimes (dilute, semidilute unentangled and semidilute entangled) is very relevant to understand the process of fiber formation from a solution rheological standpoint and the effect it has on electrospinning. While some of these issues were addressed in the previous study[33], the present study aims to further investigate and test the effects of scaling relationships between viscosity and concentration in different concentration regimes *on fiber formation and morphological features of electrospun systems.* This was done by utilizing a series that covers a relatively wider range in molecular weight, viz. 12,470 g/mol to 365,700 g/mol weight average ($M_w$) as compared to that utilized in the earlier study. In addition, *narrow ($M_w/M_n$~1.03-1.35) and relatively broader* ($M_w/M_n$~1.62-2.12) MWD linear homopolymers of poly(methylmethacrylate) (PMMA) were utilized in the present investigation. Electrospinning of all solutions in a good solvent, *N,N*-dimethyl formamide (DMF), was conducted at identical processing conditions.

**2.3 Background Theory**

For homogeneous solutions of a linear polymer, the well known Huggins Equation describes the solution viscosity[37]

$$\eta_{sp}(\mathbf{c}) = [\eta]\mathbf{c} + \mathbf{k}_{\mathbf{H}}([\eta]\mathbf{c})^2 + \ldots \quad (2.1)$$

where $\eta_{sp}(c)$ is the specific viscosity, $[\eta]$ is the intrinsic viscosity, $c$ is the polymer concentration, and $k_H$ is the Huggins coefficient. The dimensionless product of the intrinsic viscosity and the concentration, $[\eta]c$ is referred to as the Berry number, $B_e$.[38] The significance of the Berry number arises from the fact that for a solution to have chain entanglements, $B_e$>1. In dilute solutions, where polymer chains do not overlap each other (Figure 2.2a), $B_e$ can, at best, be unity ($B_e$~1). In Eq. 2.1, the intrinsic viscosity is the

initial slope of the plot between specific viscosity and concentration and is related to the root-mean-squared end-to-end distance, $<R^2>^{1/2}$, of the linear polymer chain that has $N$ monomers by the Fox-Flory relationship.[39]

$$[\eta] \sim \frac{< \mathbf{R}^2 >^{3/2}}{\mathbf{N}} \tag{2.2}$$

In addition, the intrinsic viscosity, $[\eta]$ can also be related to the molecular weight (M) of a linear polymer by the Mark-Houwink-Sakurada equation[40]

$$[\eta] = K\, \mathrm{M}^{a} \tag{2.3}$$

where the constants $K$ and $a$ depend on the polymer, solvent and temperature.[41]

The critical chain overlap concentration, c*, is the crossover concentration between the dilute and the semidilute concentration regimes. Physically, the critical chain overlap concentration is the point when the concentration inside a single macromolecular chain equals the solution concentration and can be expressed as

$$\mathbf{c^*} \sim \frac{\mathbf{N}}{< \mathbf{R}^2 >^{3/2}} \sim \frac{1}{[\eta]} \tag{2.4a}$$

From Eq. 2.4a, it is clear that $c^*[\eta] \sim 1$ in the dilute solution limit, thereby suggesting the criteria, $\mathbf{c^*} \sim 1/[\eta]$, as a means of evaluating c* (recall that this criteria is the same as that discussed above with regard to $B_e \sim 1 \Rightarrow c \sim 1/[\eta]$ in the dilute solution limit). Hence, the calculation of c* from chain dimensions:

$$\mathbf{c^*} = \frac{3\,\mathbf{M}}{4\pi < \mathbf{R}^2 >^{3/2} \mathbf{N_{av}}} \tag{2.4b}$$

in conjunction with the criteria $\mathbf{c^*} \sim 1/[\eta]$ are the two ways that can and have been utilized[42] to estimate c* (In Eq. 2.4b, $N_{av}$ is the Avogadro number and $M$ is the molecular weight). Furthermore, in a good solvent, the radius of gyration, $R_g$, is usually a better estimate of the chain dimensions than the root-mean-squared end-to-end distance, $<R^2>^{1/2}$ as it accounts for the hydrodynamic interactions between the polymer chains and the solvent. It is well established that the radius of gyration can be estimated from the hydrodynamic radius, $R_h$, (assuming non draining conditions) based on the Kirkwood-Riseman theory[40]

$$\mathbf{R_g} = \mathbf{R_h} / 0.875 \tag{2.5}$$

where the hydrodynamic radius can be determined by dynamic light scattering measurements.

In dilute solutions of good solvents, the solution viscosity has been measured experimentally[42, 43] to be proportional to the concentration, ($\eta \sim c$). This is consistent with Eq. 2.1 at *very small* values of $c$ (in the dilute regime), where the higher power terms of concentration are negligible. However, for c>c* in good solvents, de Gennes[44, 45] assumed a single parameter scaling in the semidilute regime to predict a power law dependence for the solution viscosity that is given by

$$\eta = \eta_s (c / c^*)^{3/(3\nu-1)} \tag{2.6}$$

where $\eta_s$ is the solvent viscosity and the $\nu$ is the Flory exponent (0.5 for theta solvents and 0.6 for good solvents). In good solvents, the single parameter scaling model based on the reptation model, (where the viscosity scales with molecular weight as $\eta \sim M^{3.0}$), predicts a concentration exponent of 3.75. However, experimental data[46-48] indicates a stronger dependence of viscosity on molecular weight ($\eta \sim M^{3.4}$) than that predicted by reptation theory. It has been suggested that mechanisms of relaxation other than reptation, such as contour length fluctuations,[49] might account for this observed stronger dependence. If this stronger dependence of $\eta$ on molecular weight ($\eta \sim M^{3.4}$) is taken into account, then the exponent for the concentration dependence of viscosity has been predicted to be 4.25.[49, 50] A different scaling concept, based on two parameters, was proposed by Colby et al, where an even stronger viscosity dependence on concentration was predicted ($\eta \sim c^{4.5}$) and measured experimentally ($\eta \sim c^{4.8}$).[51]

Recent work of Colby and coworkers indicates that two different power law dependences exist within the semidilute regime,[42, 43, 50-54] viz. *semidilute unentangled* and *semidilute entangled*. A physical representation of the semidilute unentangled regime is provided in Figure 2.2b, where the concentration is large enough to have some chain overlap (c>c*) but not enough to cause any significant degree of entanglement. As the concentration is further increased (semidilute entangled regime, Figure 2.2c), the topological constraints induced by the larger occupied fraction of the available hydrodynamic volume in the solution, introduce chain entanglements. Furthermore, the crossover of concentration from the *semidilute unentangled* to *semidilute entangled*

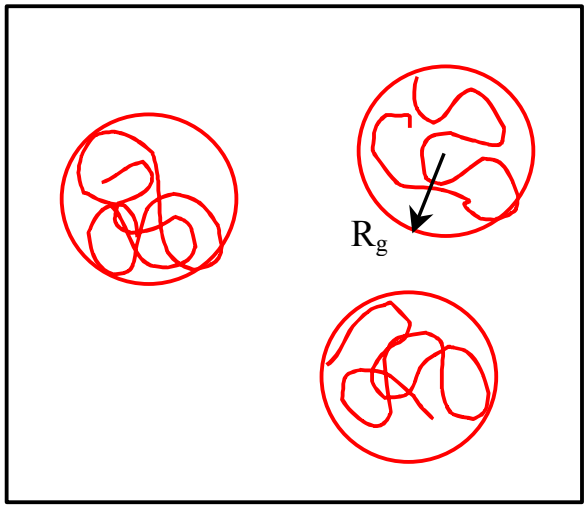


a) Dilute, $c < c^*$

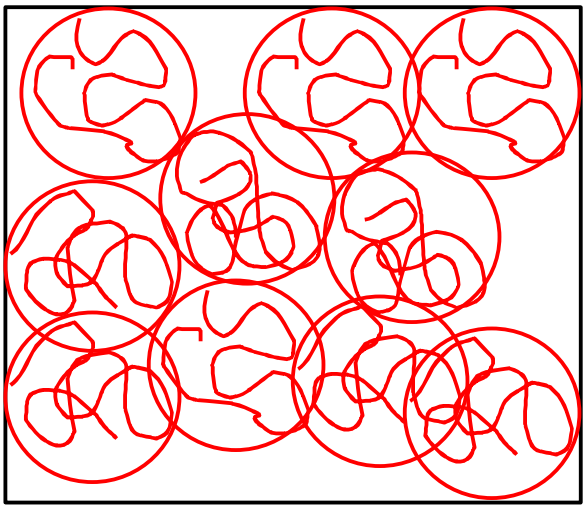

b) Semidilute unentangled, $c^* < c < c_e$

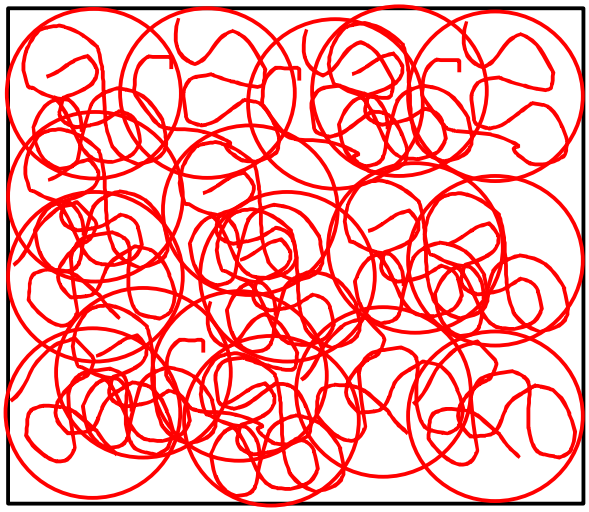

c) Semidilute entangled, $c > c_e$

**Figure 2.2** Physical representation of the three solution regimes, a) dilute b) semidilute unentangled and c) semidilute entangled.

regime is referred to as the critical entanglement concentration, $c_e$. In other words, $c_e$, marks the distinct onset of significant chain entanglements in solution. Returning to the discussion on scaling relationships in the two semidilute regimes, a weaker concentration exponent of 1.25 was predicted and experimental values in the range of 1.1-1.4 were reported in the *semidilute unentangled* regime in a good solvent.[33, 42] For *semidilute entangled* regimes, the predictions and measurements of concentration exponent are comparable to the exponents reported by de Gennes, Pearson and Colby et al (see discussion above). Thus, the *predicted* concentration exponents for the viscosity dependence in a good solvent in the semidilute regime can be summarized as:

$$\eta \sim \begin{cases} \mathbf{c}^{1.25} & \textbf{semidilute unentangled} \\ \mathbf{c}^{4.25-4.5} & \textbf{semidilute entangled} \end{cases} \tag{2.7}$$

In the present investigation, scaling relationships between viscosity and concentration in the dilute and semidilute regimes have been further investigated by utilizing solutions corresponding to molecular weights ranging from 12,470 g/mol to 365,700 g/mol $M_w$. Both the narrow ($M_w/M_n$~1.03-1.35) *and relatively broader ($M_w/M_n$ ~ 1.6-2.12) molecular weight distributions of* linear homopolymers of PMMA were utilized. Subsequent electrospinning of these solutions at identical processing conditions enabled us to determine the effects of the scaling relationships, concentration, viscosity, MW and MWD on fiber formation and morphological features of the electrospun material.

## 2.4 Experimental

### 2.4.1 Materials

For the synthesis of narrow MWD PMMA, methyl methacrylate (MMA) and 1, 1-diphenyl ethylene (DPE), procured from Aldrich®, were stirred over calcium hydride at 25 °C for 24 hours, degassed several times, and vacuum distilled (0.10 mm Hg, 23-25 °C) to remove any moisture. Methyl methacrylate was further purified by vacuum distillation from triethyl aluminum. DMF and sec-butyllithium (1.4M in cyclohexane) were also procured from Aldrich® and used without any further purification. Tetrahydrofuran (THF) was distilled under nitrogen from sodium and benzophenone immediately prior to use. Four narrow MWD PMMA grades were synthesized that had molecular weights ranging from 12,470 – 205,800 g/mol $M_w$.

In addition to the synthesized PMMA, three commercial grades (34,070, 95,850 and 365,700 g/mol $M_w$) of PMMA, that had relatively broader MWD as compared to the synthesized PMMA, were also utilized to ascertain the effect, if any, of MWD on fiber formation and morphological features of the electrospun material. These were procured from Poly Sciences® (34,070 and 95,850 g/mol $M_w$) and Aldrich® (365,700 g/mol $M_w$) and were used without any further purification.

**2.4.2 Synthesis and characterization of linear PMMA**

A series of poly(methyl methacrylate) (PMMA) homopolymers was synthesized via anionic polymerization as shown in Scheme 2.1. A 250 mL flame-dried round-bottomed flask containing anhydrous THF (100 mL, 88 mol) and DPE (0.144 g, 0.8 mmol) was cooled to -78 °C under pressurized nitrogen. Initially, sec-butyllithium was added to the solution drop by drop until a faint red color was observed, following which an additional quantity of sec-butyllithium (0.09 mL, 0.2 mmol) was added to form the initiator adduct. Freshly distilled MMA (10.7 mL, 0.1 mmol) was then added drop by drop to the initiator adduct following which the reaction was allowed to continue for 10 minutes. After 10 minutes, degassed methanol (0.25 mL, 9.9 mmol) was added to terminate the reaction following which the solution was precipitated drop by drop into a 9:1 w/w solution of methanol:water. The polymer was vacuum filtered and dried at 100 ºC under vacuum.

Molecular weights of all polymer grades (including the commercial and laboratory synthesized samples) were determined using size exclusion chromatography (SEC) using a Waters 717 Plus equipped with a Waters 2410 refractive index (RI) detector. The concentration gradient of the refractive index, *dn/dc*, was determined on-line using the calibration constant for the RI detector and the mass of the polymer sample. In addition, a Wyatt Technology Minidawn multiple angle laser light scattering (MALLS) detector was utilized to determine absolute molecular weights. All SEC measurements were performed at 40°C in THF at a flow rate of 1.0 mL/min. The molecular weights obtained from SEC agreed well with those calculated based on the grams of monomer to moles of initiator ratio. These polymers also exhibited monomodal SEC traces (data not shown here). $^1$H NMR spectra were determined in $CDCl_3$ at 400

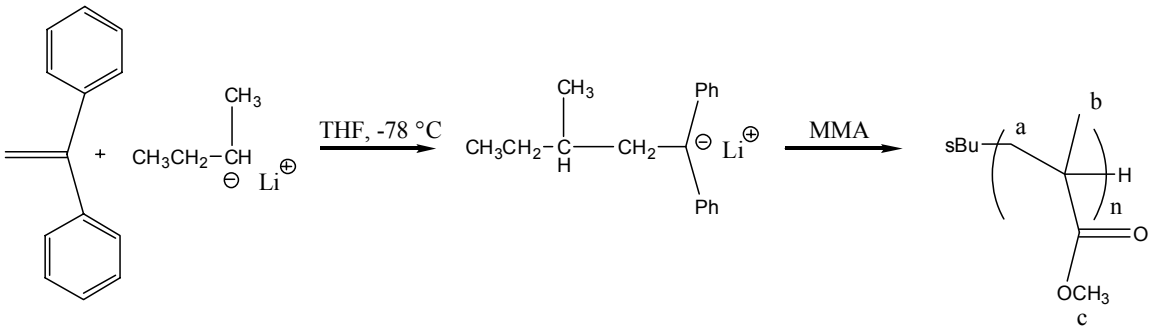


**Scheme 2.1** Scheme for the anionic polymerization of methyl methacrylate.

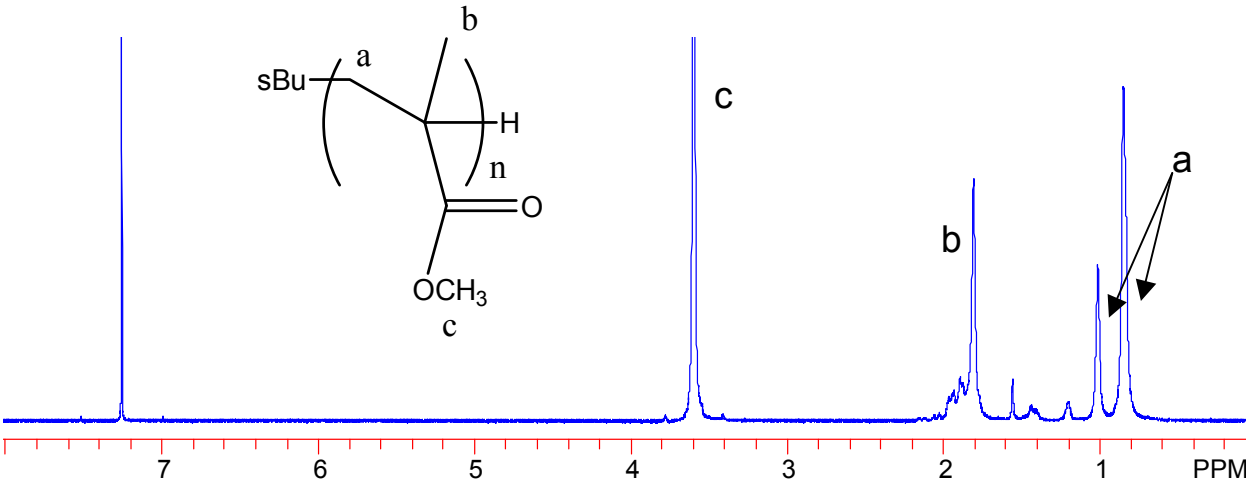


**Figure 2.3** Representative 1H NMR spectrum of anionically polymerized PMMA.

MHz with a Varian Unity Spectrometer. All peaks were well-assigned, confirming the synthesis of homopolymers of PMMA (Figure 2.3).

The molecular weights and molecular weight distribution for the series of polymers are summarized in Table 2.1. The synthesized polymers had a weight average

**Table 2.1** Molecular weight, calculated intrinsic viscosity from Mark Houwink parameters, hydrodynamic radius, radius of gyration and critical chain overlap concentration, c*, of synthesized and commercial grades of PMMA. Note the comparison between the c* estimated from the intrinsic viscosity and the c* calculated from the chain dimensions obtained from dynamic light scattering measurements at 25 oC in DMF. The c* values are converted to wt% by utilizing the specific gravity of DMF at 25 $^{o}$C to be 0.95 g/cc.

| $M_w$ | $M_n$ | $M_w/M_n$ | $K_w$=0.015 cm$^3$/g, a = 0.667$^{\dagger}$ | | | Light scattering | | C* | C* |
|---|---|---|---|---|---|---|---|---|---|
| g/mol | g/mol | | [η] in DMF | C*~1/[η] | C* | $R_h$ | $R_g$ | g/cm$^3$ | wt% |
| | | | cm$^3$/g | g/cm$^3$ | wt% | nm | nm | | |
| **Synthesized** | | | | | | | | | |
| 12,470 | 12,060 | 1.03 | 8.1 | 0.124 | 11.5 | 2.30 | 2.6 | 0.107 | 10.2 |
| 17,710 | 17,200 | 1.03 | 10.2 | 0.098 | 9.3 | 2.50 | 2.9 | 0.119 | 11.2 |
| 125,900 | 100,300 | 1.26 | 37.8 | 0.026 | 2.7 | 7.00 | 8.0 | 0.032 | 3.3 |
| 205,800 | 152,500 | 1.35 | 52.5 | 0.019 | 2.0 | 8.80 | 10.1 | 0.024 | 2.5 |
| **Commercial** | | | | | | | | | |
| 34,070 | 21,000 | 1.62 | 15.8 | 0.063 | 6.2 | 3.30 | 3.7 | 0.065 | 6.4 |
| 95,850 | 45250 | 2.12 | 31.5 | 0.032 | 3.2 | 5.2 | 5.9 | 0.035 | 3.5 |
| 365,700 | 207,300 | 1.76 | 77.0 | 0.013 | 1.3 | 10.70 | 12.3 | 0.018 | 1.9 |

$^{\dagger}$The values of Mark Houwink parameters, *K* and *a* were obtained from the literature.[57]

molecular weights ($M_w$) ranging from 12,470 – 205,800 g/mol with MWD in the range of 1.03-1.35. In comparison, the commercial grades of PMMA ($M_w$ of 34,070, 95,800 and 365,700 g/mol procured from Aldrich® and Polysciences®) were relatively broader ($M_w/M_n$ ~ 1.6-2.12). The MW and MWD of commercial polymers are also listed in Table 2.1.

### 2.4.3 Dynamic Light Scattering (DLS) on PMMA solutions to estimate chain dimensions

Dilute solutions corresponding to each MW grade of PMMA (0.5-1 wt%) were prepared in DMF at 25 $^{o}$C. These solutions were utilized for DLS measurements that were conducted on a DynaPro®-E-50830 equipped with a DynaPro® TC100-830

temperature controller. All measurements were made with a 826.3 nm laser at 25 $^{o}$C at a fixed angle of 90$^{o}$. Comprehensive treatments of the theory of dynamic light scattering can be found elsewhere.[55, 56] Briefly, the measured autocorrelation function was fitted with an exponential curve to obtain the diffusion coefficient, which was subsequently utilized to calculate the hydrodynamic radius via the Stokes-Einstein equation. The radius of gyration was then calculated by Eq. 2.5, described in section 2.3.

**2.4.4 Electrospinning and characterization**

Based on the $R_g$ values measured from DLS, c* was calculated (Eq. 2.4b) for each of the laboratory synthesized and commercial grades of MW utilized in this study. Keeping these c* values in consideration, solutions were made in DMF at 25 $^{o}$C at different concentrations to span the dilute, semidilute unentangled and semidilute entangled regimes. Prior to electrospinning, the viscosities of these solutions were measured with an AR-1000 Rheometer (TA Instruments Inc.). The steady state viscosity measurements were performed in the continuous ramp mode at room temperature (25 $^{o}$C) using cone and plate geometry. The sample solution was placed between the fixed Peltier plate and a rotating cone (diameter: 4 cm, vertex angle: 2$^{o}$) attached to the driving motor spindle. The changes in viscosity and shear stress with change in shear rate were measured. A computer interfaced to the equipment recorded the resulting shear stress vs. shear rate data. All the solutions investigated in this study displayed shear thinning behavior at high shear rates (viscosity-shear rate curves not shown). The initial slope of the plot of the shear stress-shear rate data where Newtonian behavior was observed gave the zero shear viscosity, $\eta_o$. As expected, the Newtonian shear rate range was suppressed with increasing concentration. For dilute and semidilute unentangled solutions ($c/c^* < 3$), Newtonian behavior was observed in the range of 0-3000 $s^{-1}$. Solution viscosity of *dilute* solutions of lower $M_w$ of 12,470 and 17,710 g/mol could not be recorded due to immeasurable shear stresses generated at maximum attainable shear rates in the cone-plate geometry. For the semidilute entangled solutions ($3<c/c^*<6$), Newtonian behavior was observed in the shear rate range of 0-1000 $s^{-1}$ and for relatively concentrated solutions ($c/c^*>6$), the Newtonian shear rate range was observed only up to 100 $s^{-1}$.

Electrospinning of these same solutions was done on an apparatus depicted earlier in Figure 2.1. The syringe containing the polymer solution was connected to a Teflon

needle (0.7 mm internal diameter). A platinum electrode, placed in the syringe that was immersed in the polymer solution, was connected to a high voltage DC supply at a positive polarity. A syringe-pump connected to the wide-end of the syringe controlled the flow rate emanating out of the Teflon needle tip. Electrospun materials were collected on a grounded steel wire mesh that served as the target, and was kept at 15 cm from the Teflon tip. The diameter of the steel wire mesh was ca. 0.5 mm with a mesh count of 20x20 (20 steel wires per 1" each in the horizontal and vertical axes). All solutions were electrospun at 25 $^{o}$C, 10 kV, 3ml/h with a 15 cm separation distance between the target and Teflon tip.

Post-spinning characterization of the morphology of the electrospun material collected on the steel wire mesh target was done using a Leo® 1550 Field Emission Scanning Electron Microscope (FESEM). A Cressington® 208HR sputter-coater was utilized to sputter-coat the electrospun fiber samples with a 5 nm Pt/Au layer to minimize electron charging effects.

## 2.5 Results and Discussion

### 2.5.1 Determination of c* and scaling exponents in the two semidilute concentration regimes

As discussed in section 2.3, the intrinsic viscosity of a polymer can be related to its MW by the Mark-Houwink-Sakurada relationship, Eq. 2.3. Dobkowski[57] measured the intrinsic viscosity of a series of PMMA polymers ($M_w/M_n$ ~ 1.0-1.6) to determine the values of the Mark-Houwink parameters, *K* and *a* at 25 $^{o}$C in DMF. These were reported as 0.015 g/cm$^3$ and 0.667 respectively at conditions identical to those employed for electrospinning (25 $^{o}$C in DMF) in the present investigations. Based on these parameters, the estimated intrinsic viscosities corresponding to each MW grade are listed in Table 2.1. The critical chain overlap concentration, or c*, was then *theoretically calculated* by the criteria $\mathbf{c}^*[\eta] \sim 1$, discussed earlier in section 2.3. These are reported in Table 2.1 along with the converted values to wt% (taking the specific gravity of DMF as 0.95 g/cm$^3$). It can be seen that c* decreases with increasing molecular weight as the lower molecular weight chains, that have lower occupied hydrodynamic volume, require a higher concentration to overlap, as is expected. The values of chain dimensions (from DLS) and the *experimentally calculated* c* are also reported in Table 2.1. It is noted that

the theoretically calculated values of c* are generally in good agreement with the corresponding experimentally calculated values for each MW grade investigated in this study.

The variation of the zero shear viscosity of different solutions as a function of concentration is shown in Figure 2.4 for the PMMA grades. Within the range of concentrations investigated, the variation in the slope with concentration was distinctly observed. Recall that the viscosities of dilute solutions of the lowest $M_w$ of 12,470 and 17,710 g/mol, could not be measured and are thus not a part of Figure 2.4. To facilitate better interpretation, the viscosity was replotted with the concentration rescaled by the experimentally determined values of c* (corresponding to each MW), as shown in Figure 2.5. Beyond the *dilute regime,* that extends until *c/c*~1*, two distinct regimes were observed as indicated by the change in the slope of the trend in the data. Based on the literature,[42, 43, 50-54] these two regimes correspond to the *semidilute unentangled* and *semidilute entangled* respectively. In the present investigation, the crossover between the two regimes takes place at c/c*~3 which marks the onset of the critical chain overlap concentration, $c_e$, (as discussed in section 2.3), where the polymer chains topologically constrain each other and begin to entangle. Returning to Figure 2.5, the concentration exponent in the semidilute unentangled regimes is *0.65 ($R^2$=0.96)*, which indicates a weaker dependence than the predicted value of 1.25. However, the concentration exponent in the semidilute entangled regime is 5.3 which, while a bit high, is close to the predicted range (4.25-4.5) and quite comparable to that observed by Colby et al[51] (4.8).

### 2.5.2 Fiber formation during electrospinning

#### 2.5.2.1 Electrospinning of solutions in the *dilute* concentration regime

The FESEM results of electrospinning PMMA from dilute solutions (c/c*<1) are shown in Figure 2.6. For all the polymer grades electrospun from solution concentrations below c*, insufficient chain overlap lead to the formation of polymer droplets (micrographs corresponding to all the polymers are not shown in Figure 2.6 for the sake of brevity).

#### 2.5.2.2 Electrospinning of solutions in the *semidilute* concentration regime

As the solution concentration was increased above c* but less than $c_e$ (in the semidilute unentangled regime, 1<c/c*<3), the observed morphology was dependent on

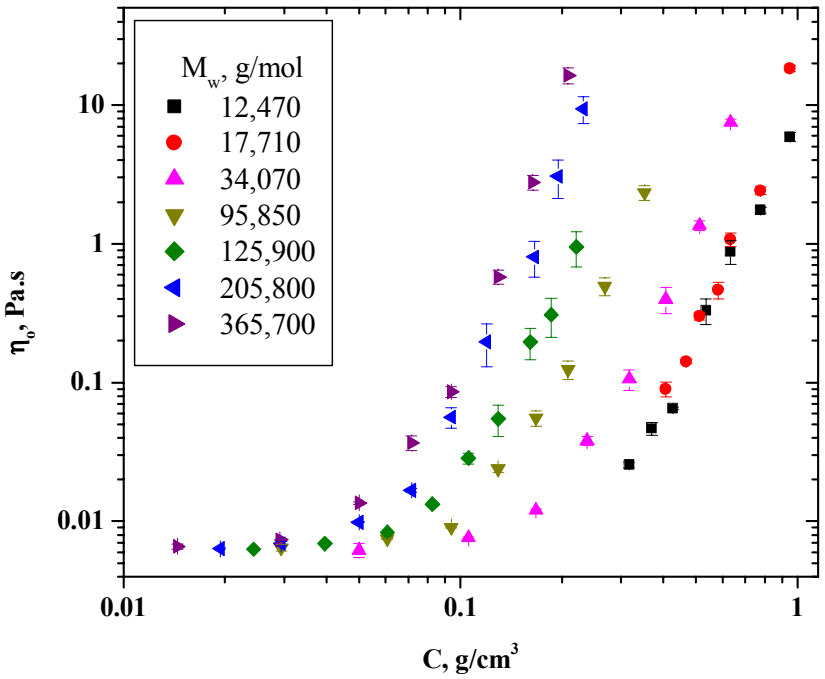


**Figure 2.4** Plot of zero shear rate viscosity, $\eta_o$, with concentration for the different MW grades of PMMA.

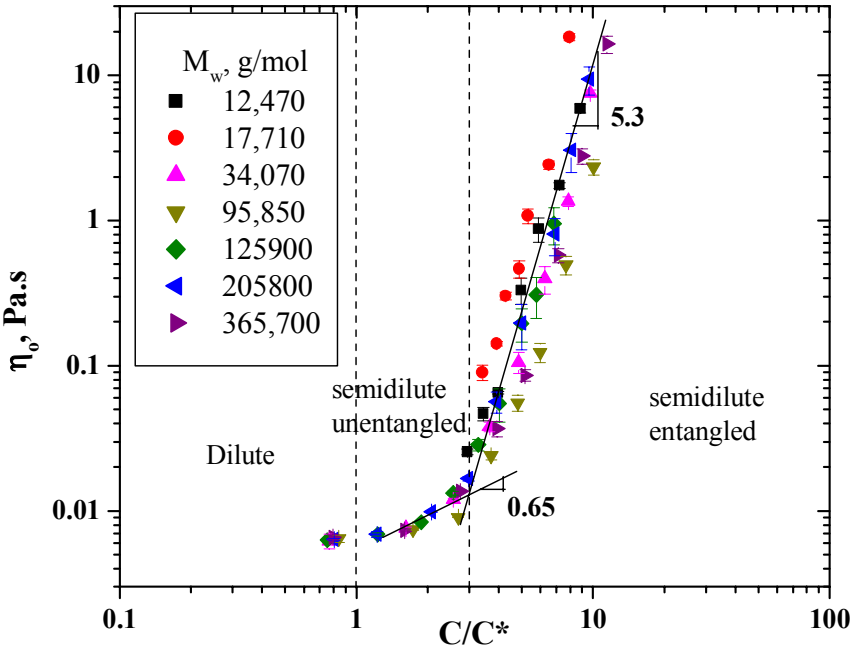


**Figure 2.5** Plot of zero shear rate viscosity, $\eta_o$, with c/c* for the different MW grades of PMMA

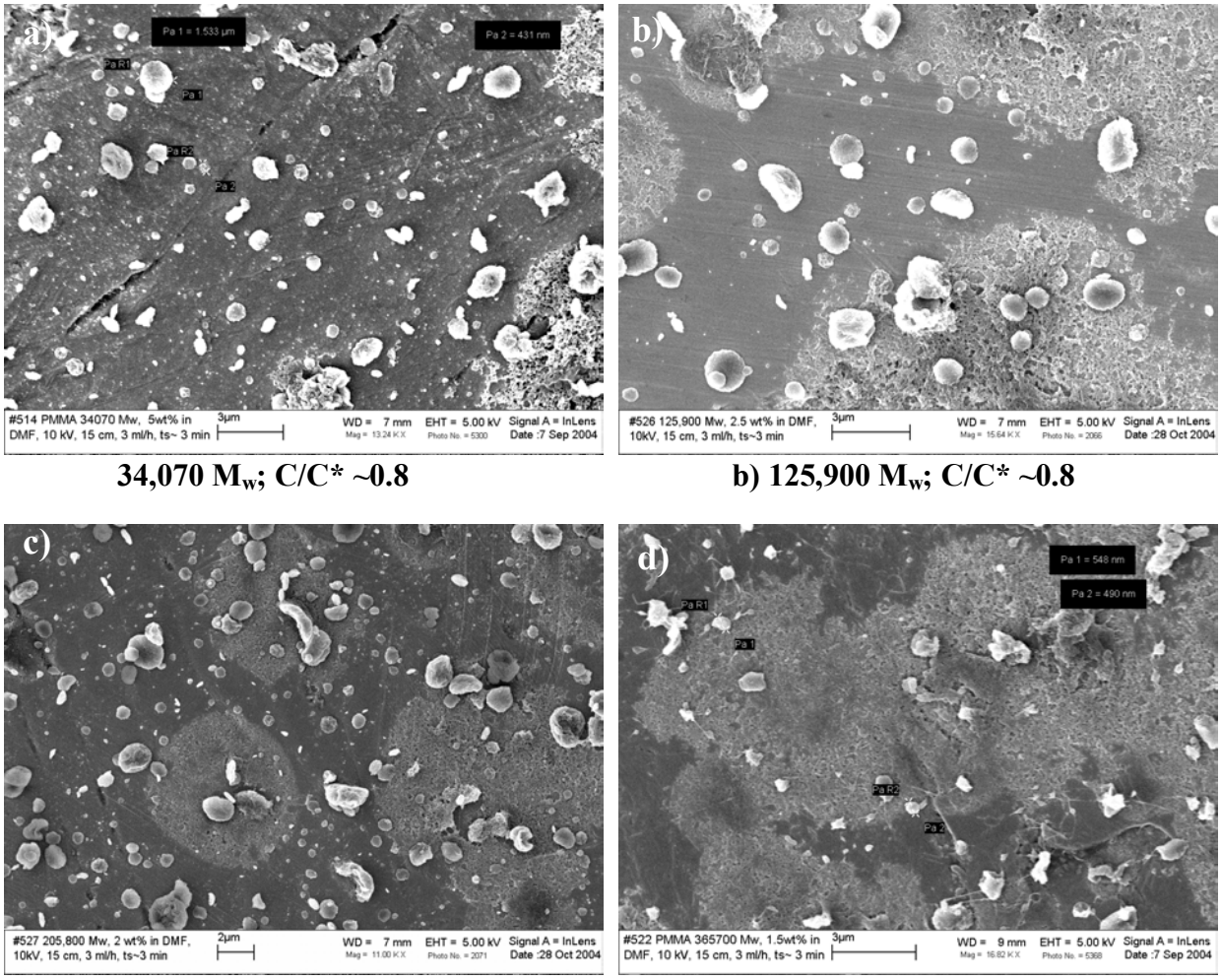


**34,070 $M_w$; C/C* ~0.8** **b) 125,900 $M_w$; C/C* ~0.8**

**205,800 $M_w$; C/C* ~0.8** **365,700 $M_w$; C/C* ~0.8**

Figure 2.6 SEM Micrographs of PMMA electrospun from solutions in the *dilute regime,* c/*c*<1*. Insufficient chain overlap at solution concentrations below c* leads to the formation of polymer droplets.

molecular weight. At c/c*~2.6-2.9 (Figure 2.7a-c), which is at a concentration range just below $c_e$, polymer droplets were observed for the two lower molecular weights, viz. 12,470 and 17,710 g/mol $M_w$, indicating insufficient chain overlap (results corresponding to $M_w$ of 17,710 g/mol not shown here for the sake of brevity). However, with increasing molecular weight (at $M_w$ of 125,900 g/mol), in addition to polymer droplets, some limited fiber formation occurred in the form of thin fibers that were connected by polymer droplets (analogous to 'beads on a string', also often referred to as 'beaded fiber

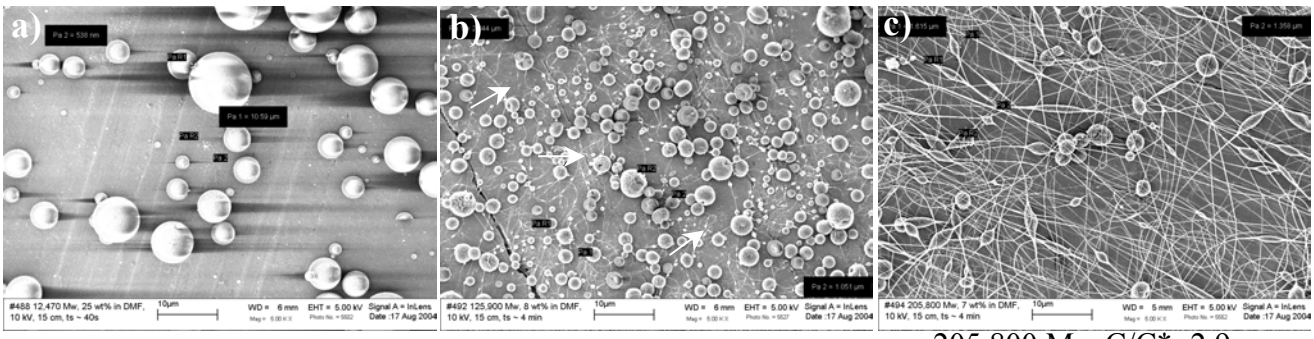


12,470 $M_w$; C/C*~2.9 125,900 $M_w$; C/C*~2.6 205,800 $M_w$; C/C*~2.9

**1<c/c*<3, semidilute unentangled**

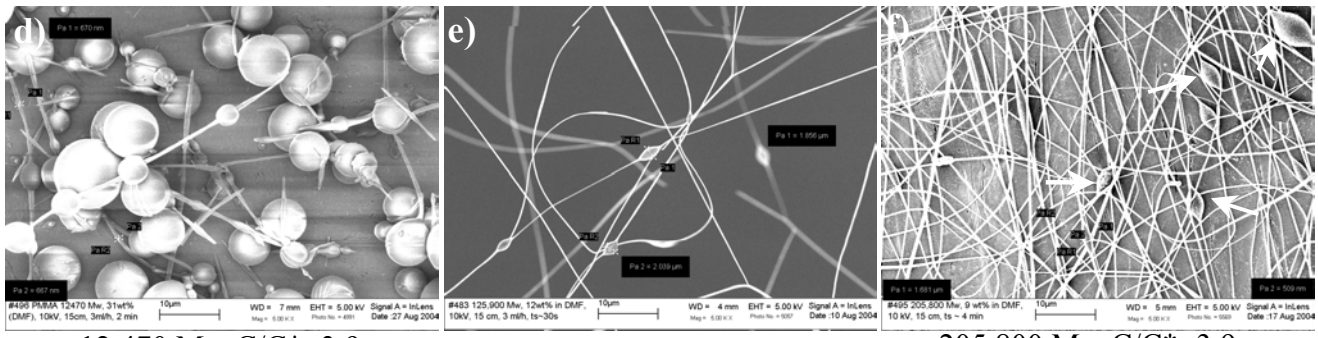


12,470 $M_w$; C/C*~3.9 125,900 $M_w$; C/C*~4.0 205,800 $M_w$; C/C*~3.9

**3<c/c*<6, semidilute entangled**

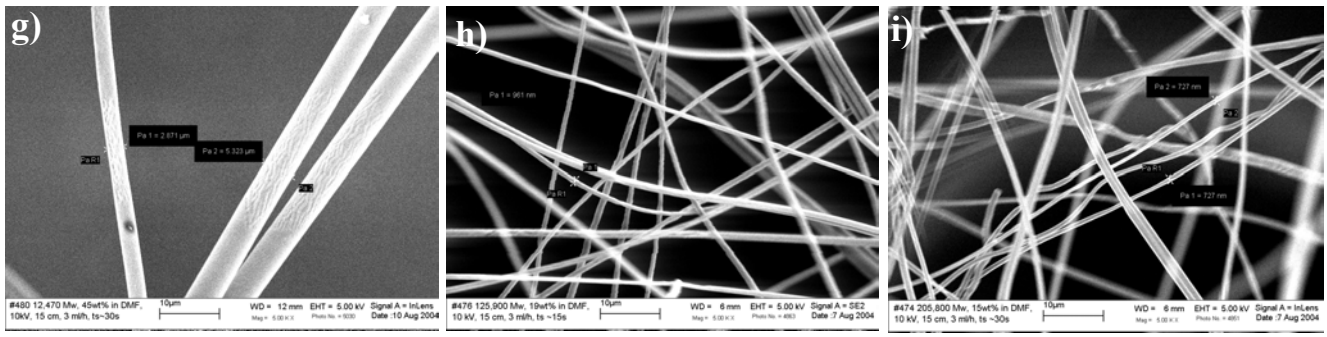


12,470 $M_w$; C/C*~7.2 125,900 $M_w$; C/C*~6.8 205,800 $M_w$; C/C*~6.8

**c/c*>6, semidilute entangled**

Figure 2.7 SEM Micrographs of PMMA electrospun from solutions in the *semi-dilute unentangled* and *entangled regimes* for the three synthesized MW grades 12,470, 125,900 and 205,800. All micrographs have the same magnification and the scale bars in the micrographs correspond to 10 μm.

morphology'[2,58]) was observed. These beaded fibers are marked by white arrows in Figure 2.7b, where the diameter of the fiber between the beads was ca. 100 nm. However, these beaded fibers were discontinuous with an overall length of no more than 10 μm. It should be noted that the formation of beaded fibers is governed by the balance between the viscosity and surface tension.[2] For low molecular weight liquids, an electrically driven jet undergoes a capillary breakdown into droplets that is driven by surface tension,[59] a phenomena also referred to as electrospraying. However, in the case of polymer solutions, the pattern of capillary breakup is quite different. Instead of the jet breakup due to the capillary instability, the jet between the droplets forms a nanofiber while the surface tension contracts the radius of the jet, thereby causing the remaining solution to form a bead.[2] Therefore as the molecular weight (and consequently the viscosity) was increased (205,800 and 365,700 g/mol), the beads and droplets became less numerous, while the distance between the beads became larger and the fiber diameter became more uniform. This can be attributed to the increased viscous and topological constraints caused by the higher occupied hydrodynamic volume of the larger MW chains that tend to resist contraction in the jet. Returning to the data in Figure 2.7, the electrospinning results from solution concentrations in the *semidilute entangled* regime at c/c*~3.9-4.0, which is at a concentration range just above $c_e$ (recall that $c_e$~3c/c*) are shown in Figures 2.7d-f. At a $M_w$ of 12,470 g/mol (Figure 2.7d) and 17,710 g/mol (results for 17,710 g/mol not shown here for the sake of brevity), polymer droplets and beaded fibers were observed to form. It was noted that the length of the fibers between the beads was no more than 20 –30 μm indicating that continuous fibers were not formed. In other words, at a molecular weight and concentration of 12,470 g/mol $M_w$ and c/c*~3.9 respectively, the chain overlap was barely sufficient to induce fiber formation. At a similar c/c* ratio (~3.9-4.0), continuous beaded fibers were observed to form at the higher $M_w$ of 125,900 g/mol (Figure 2.7e), 205,800 g/mol (Figure 2.7f) and 365,700 g/mol (results not shown for the sake of brevity). As the concentration was further increased (c/c*>6) (Figures 2.7g-i), uniform and bead free fibers were observed for all the synthesized polymers (ranging from 12,470 -205,800 g/mol $M_w$ - results for 17,710 g/mol $M_w$ not shown for the sake of brevity).

### 2.5.2.3 Effect of MWD on fiber formation

Figure 2.8 shows the results on narrow and broad MWD polymers that were electrospun at a c/c* ratio of ca. 4.8-4.9. Continuous beaded fibers were formed when solutions corresponding to a $M_w$ of 12,470 and 17,710 g/mol were electrospun (Figures 2.8a & b). However, *polymer droplets* and *some* thin and discontinuous beaded fibers were observed to form when solutions corresponding to the relatively broad MWD but higher MW polymers of $M_w$ of 34,070 and 95,850 g/mol were electrospun (Figures 2.8c & d). Furthermore, for the broad MWD polymers of $M_w$ of 34,070 and 95,850 g/mol, uniform and bead-free fibers were observed to form at c/c*~9.7 and c/c*~10.1 respectively. In contrast, recall that uniform fibers were electrospun at c/c*>6 for solutions corresponding to all the synthesized polymers ($M_w/M_n$~1.03-1.35) that had a relatively narrower MWD. These observations indicate that the onset of uniform fiber formation in relatively broader MWD polymers occurs at a higher concentration as compared to that in the narrow MWD polymers. This can be rationalized by means of the following hypothesis: in a narrow MWD ($M_w/M_n$~1.03) or monodisperse polymer, all the polymer chains in solution have nearly the same hydrodynamic volume that results in a very sharp spectrum of the relaxation times which is critical to the plastic stretching process induced by the electrically driven bending instabilities[11] during electrospun fiber formation process. Contrast this to a relatively broad MWD polymer that has a wide distribution of the hydrodynamic radii (small and large) and relaxation times (fast and slow) of the chains in solution. During the process of the plastic stretching, the presence of the relatively small polymer chains that have a smaller hydrodynamic volume and consequently a lower local chain entanglement density, acts as a weak link that causes a premature breakup of local "chain-chain coupling" within the jet resulting in the formation of polymer droplets (Figure 2.8c & d). As a result, a higher concentration and consequently higher viscosity is needed to attain sufficient entanglement density to allow uniform fiber formation at the relatively broader MWD polymer when compared to the narrow MWD analog having an equivalent $M_w$. This is exactly what was observed in the present investigation, where uniform fiber formation was observed at higher c/c*(~10) from the broader MWD polymers than the relatively narrow MWD polymers (c/c*~6).

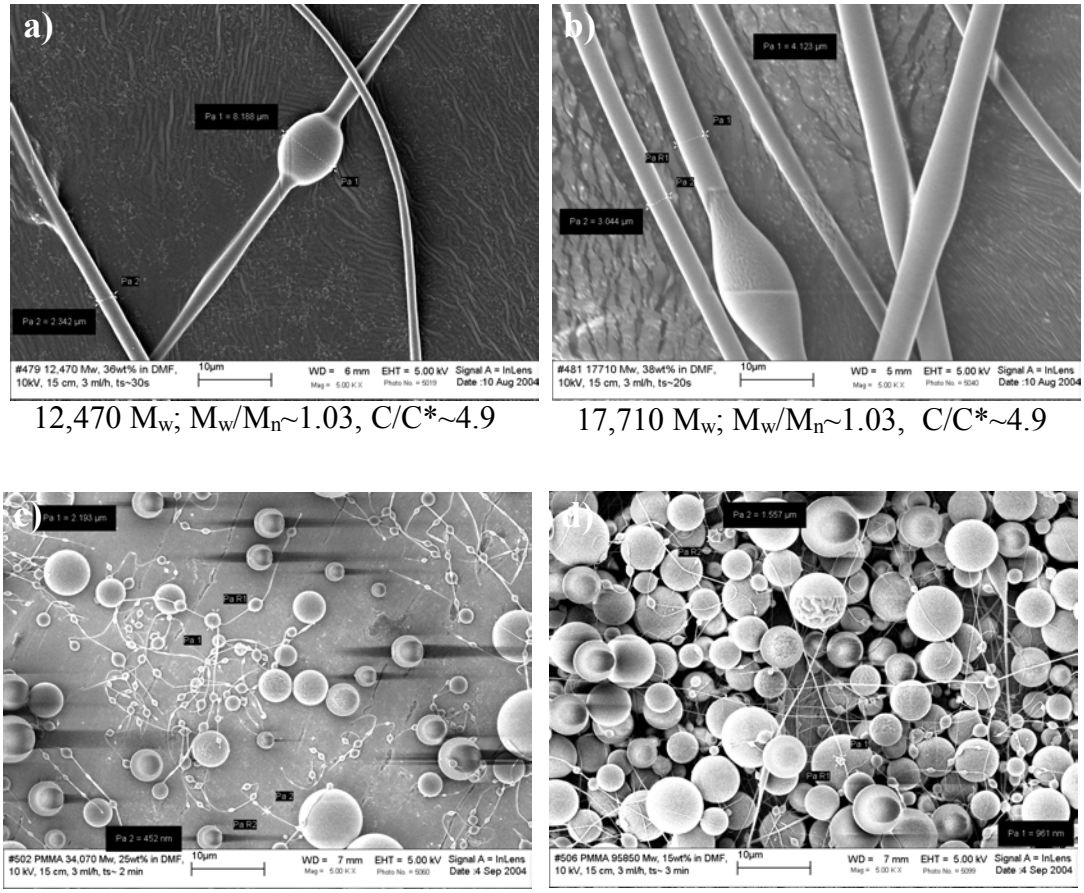


**Figure 2.8** SEM Micrographs of PMMA electrospun from solutions in the *semidilute entangled regime at c/c* ~4.8-4.9* for the narrow and broad $M_W/M_n$ polymers. All micrographs have the same magnification and the scale bars in the micrographs correspond to 10 μm.

Based on these observations, it is pertinent to investigate polymers of the same $M_w$ but different $M_w/M_n$ to study the effect of polydispersity on electrospun fiber formation. While the present study did not critically address this effect (due to the limitations in synthesizing very broad MWD, $M_w/M_n$~4+, from anionic or free radical polymerization techniques), it is suggested that such detailed investigations be conducted using an appropriate linear system that permits a wider range of MWD.

### 2.5.3 Scaling of electrospun fiber diameter on concentration and viscosity

Figure 2.9 shows the variation of the fiber diameter, including the diameter between the beads (for beaded morphology) and diameter of the uniform fibers, with c/c*. Similar to the approach utilized in the earlier study by McKee et al.,[33] linear regression of the data was conducted to estimate and compare the scaling exponent for the fiber diameter dependence on c/c*. This was found as:

$$\textbf{fiber diameter} \sim (\mathbf{c}/\mathbf{c}^*)^{3.1} \tag{2.8}$$

The scaling exponent of 3.1 indicates a somewhat stronger dependence than that observed (2.6) by the work of McKee et al reported earlier[33]. This difference may arise from the fact that in the earlier study branched and linear copolymers of PET-co-PEI were utilized whereas in the present study we have focused our investigations on only linear homopolymers of PMMA.

The fiber diameter was also found to correlate with the zero shear viscosity of the semidilute solutions, as shown in Figure 2.10. This data indicates a direct correlation between the fiber diameter and the zero shear viscosity. It is important to note that individual data points in each of the series corresponding to $M_w$ of 12,470, 17,710, 34,070 and 95,850 g/mol display a linear relationship, whereas the data points in the higher MW series ($M_w$ of 125,900, 205,800 and 365,700 g/mol) do not display a linear relationship. It appears that a linear correlation exists only up to a MW of ca. 100,000 g/mol. The linear regression on the data corresponding to the four series ($M_w$ of 12,470, 17,710, 34,070 and 95,850 g/mol) gave,

$$\textbf{fiber diamter} \sim \eta_0^{0.72} \tag{2.9}$$

with $R^2$ = 0.93. Interestingly, this was found to be in close agreement with the relationship reported earlier by the work of McKee et al[33] (*fiber diameter* ~ $\eta_o^{0.8}$) where investigations on branched and linear copolymers of PET-co-PEI that had $M_w$ values in the range of 11,700-106,000 g/mol were conducted, a MW range similar to that utilized for linear regression in Eq. 2.9. Linear regression of the fiber diameter vs. viscosity data corresponding to *all* the seven molecular weights (ranging from 12,470 – 365,700 g/mol Mw) resulted in the: *fiber diameter* ~ $\eta_o^{0.71}$ with a $R^2$ value of 0.91, thereby indicating no significant change in the scaling exponent. It is important to note, however, that the extensional viscosity of the jet, while in flight to the target is undoubtedly very influential

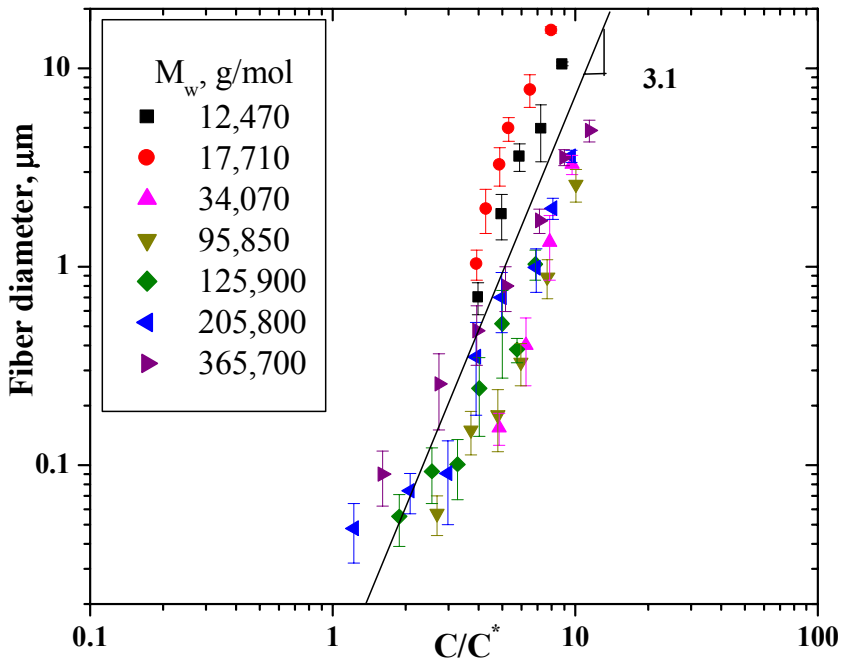


**Figure 2.9** Variation of fiber diameter with c/c* for the different MW grades of PMMA.

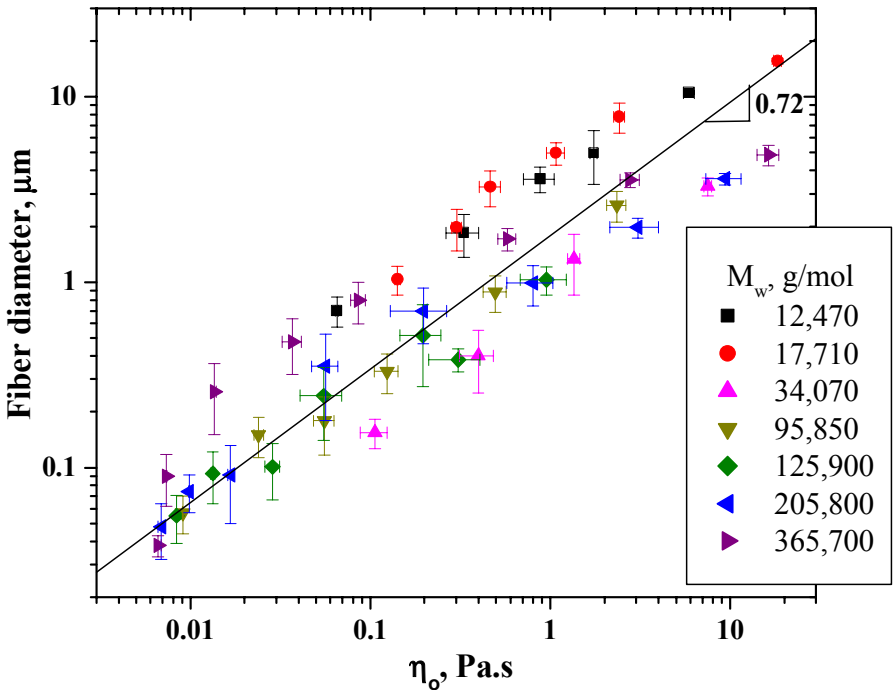


**Figure 2.10** Variation of fiber diameter with zero shear rate viscosity for the different MW grades of PMMA.

in governing the stretching induced in the jet, which in turn affects the final diameter of the polymer filament. However, to the authors' knowledge, a thorough study of the effect of extensional viscosity on fiber formation in electrospinning has not been reported to date, although such a study would certainly be warranted.

**2.6 Conclusions**

A series of seven linear homopolymers of PMMA ranging from 12,470 – 365,700 g/mol $M_w$, were utilized to explore scaling relationships between the viscosity and concentration in semidilute regimes in a good solvent to investigate fiber formation during electrospinning. Chain dimensions of these polymers in DMF at 25 $^oC$ were measured by dynamic light scattering to estimate the critical chain overlap concentration, c*. For each of the polymers investigated, the experimentally determined value of c* was in good agreement with the theoretically determined value, estimated by the criteria $\mathbf{c^*} \sim 1/[\eta]$, where the intrinsic viscosity was estimated from the Mark-Houwink parameters, *K* and *a* (at 25 $^oC$ in DMF) obtained from the literature. The plot of the zero shear viscosity with the c/c* distinctly separated into different solution regimes, viz., dilute (c/c*<1), semidilute unentangled (1<c/c*<3) and semidilute entangled (c/c*>3). The crossover between semidilute unentangled and semidilute entangled concentration regimes was observed at c/c*~3, which therefore marked the onset of the critical chain overlap concentration, $c_e$. Electrospinning of all solutions was done at identical conditions to ascertain the effects of solution concentration on fiber formation and morphological features of the electrospun material. Electrospinning of dilute solutions resulted in the formation of polymer droplets due to insufficient chain overlap between the chains. As the concentration was increased (semidilute unentangled regime 1<c/c*<3), polymer droplets and *some* beaded fibers were observed. Upon further increase in concentration (semidilute entangled regime), beaded fibers were obtained at 3<c/c*<6. Uniform fiber formation was observed at c/c*~6 for all the narrow MWD ($M_w/M_n$~1.03-1.35) polymers but for the relatively broad MWD polymers of $M_w$ of 34,070 ($M_w/M_n$ ~ 1.62) and 95,800 ($M_w/M_n$ ~ 2.12) g/mol, uniform fibers were formed at much higher concentrations, viz. c/c*~9.7 and 10.1 respectively. Dependence of fiber diameter on concentration was determined, viz., $fiber\ fiber\ dia \sim (c/c^*)^{3.1}$. The fiber

diameter was also found to vary with the zero shear viscosity of the solutions as, *fiber dia* $\sim \eta_o^{0.71}$.

**Acknowledgements**

This material is based upon work supported by, or in part by, the U.S. Army Research Laboratory and the U.S. Army Research Office under grant number DAAD19-02-1-0275 Macromolecular Architecture for Performance (MAP) MURI. The author thanks Prof. Tim Long and Casey Elkins, Chemistry Department, Virginia Tech for the synthesis of PMMA polymers utilized in this investigation and Prof. Chip Frazier, Wood Science Department, Virginia Tech, for allowing the use of AR-1000 Rheometer for viscosity measurements. Thanks to Prof. Alan Esker, Chemistry Department, Virginia Tech, for allowing the use of Light scattering equipment for hydrodynamic radius measurements and Prof. Richey Davis, Chemical Engineering Department, Virginia Tech, for the meaningful discussions and guidance on the dynamic light scattering theory and measurements.

**References**

(1) Doshi, J.; Reneker, D. H. *Journal of Electrostatics* **1995**, *35*, 151-160.

(2) Fong, H.; Chun, I.; Reneker, D. H. *Polymer* **1999**, *40*, 4585-4592.

(3) Kim, J.-S.; Reneker, D. H. *Polymer Engineering and Science* **1999**, *39*, 849-854.

(4) Deitzel, J. M.; Kleinmeyer, J. D.; Hirvonen, J. K.; Beck Tan, N. C. *Polymer* **2001**, *42*, 8163-8170.

(5) Srinivasan, G.; Reneker, D. H. *Polymer International* **1995**, *36*, 195-201.

(6) Koombhongse, S., 2001.

(7) Koombhongse, S.; Liu, W.; Reneker, D. H. *Journal of Polymer Science, Part B: Polymer Physics* **2001**, *39*, 2598-2606.

(8) Schreuder-Gibson, H. *International Conference on Textile Coating & Laminating: Preparing for the Future--A New Millenium, 8th, Frankfurt, Germany, Nov. 9-10, 1998* **1998**, Paper No17/11-Paper No17/24.

(9) Matthews, J. A.; Wnek, G. E.; Simpson, D. G.; Bowlin, G. L. *Biomacromolecules* **2002**, *3*, 232-238.

(10) Matthews, J. A.; Boland, E. D.; Wnek, G. E.; Simpson, D. G.; Bowlin, G. L. *Journal of Bioactive and Compatible Polymers* **2003**, *18*, 125-134.

(11) Reneker, D. H.; Yarin, A. L.; Fong, H.; Koombhongse, S. *Journal of Applied Physics* **2000**, *87*, 4531-4547.

(12) Yarin, A. L.; Koombhongse, S.; Reneker, D. H. *Journal of Applied Physics* **2001**, *90*, 4836-4846.

(13) Yarin, A. L.; Koombhongse, S.; Reneker, D. H. *Journal of Applied Physics* **2001**, *89*, 3018-3026.

(14) Hohman, M. M.; Shin, M.; Rutledge, G.; Brenner, M. P. *Physics of Fluids* **2001**, *13*, 2221-2236.

(15) Hohman, M. M.; Shin, M.; Rutledge, G.; Brenner, M. P. *Physics of Fluids* **2001**, *13*, 2201-2220.

(16) Ziabicki, A. *In Fundamentals of Fiber Formation.*; Wiley Interscience: NY, 1976.

(17) Wang, X.; Lee, S.-H.; Drew, C.; Senecal, K. J.; Kumar, J.; Samuelson, L. *Abstracts of Papers, 222nd ACS National Meeting, Chicago, IL, United States, August 26-30, 2001* **2001**, PMSE-366.

(18) Lee, S.-H.; Ku, B.-C.; Wang, X.; Samuelson, L. A.; Kumar, J. *Materials Research Society Symposium Proceedings* **2002**, *708*, 403-408.

(19) Zhang, Y.; Dong, H.; Norris, I. D.; MacDiarmid, A. G.; Jones, W. E., Jr. *Abstracts of Papers, 222nd ACS National Meeting, Chicago, IL, United States, August 26-30, 2001* **2001**, PMSE-369.

(20) Fong, H.; Liu, W.; Wang, C.-S.; Vaia, R. A. *Polymer* **2001**, *43*, 775-780.

(21) Deitzel, J. M.; Kosik, W.; McKnight, S. H.; Tan, N. C. B.; DeSimone, J. M.; Crette, S. *Polymer* **2002**, *43*, 1025-1029.

(22) Boland, E. D.; Bowlin, G. L.; Simpson, D. G.; Wnek, G. E. *Abstracts of Papers, 222nd ACS National Meeting, Chicago, IL, United States, August 26-30, 2001* **2001**, PMSE-031.

(23) Boland, E. D.; Matthews, J. A.; Pawlowski, K. J.; Simpson, D. G.; Wnek, G. E.; Bowlin, G. L. *Frontiers in Bioscience* **2004**, *9*, 1422-1432.

(24) Boland, E. D.; Simpson, D. G.; Wnek, G. E.; Bowlin, G. L. *Polymer Preprints (American Chemical Society, Division of Polymer Chemistry)* **2003**, *44*, 92-93.

(25) Boland, E. D.; Simpson, D. G.; Wnek, G. E.; Bowlin, G. L. *Abstracts of Papers, 226th ACS National Meeting, New York, NY, United States, September 7-11, 2003* **2003**, POLY-533.

(26) Boland, E. D.; Wnek, G. E.; Simpson, D. G.; Pawlowski, K. J.; Bowlin, G. L. *Journal of Macromolecular Science, Pure and Applied Chemistry* **2001**, *A38*, 1231-1243.

(27) Boland Eugene, D.; Matthews Jamil, A.; Pawlowski Kristin, J.; Simpson David, G.; Wnek Gary, E.; Bowlin Gary, L. *Frontiers in bioscience : a journal and virtual library* **2004**, *9*, 1422-1432.

(28) Kenawy, E.-R.; Bowlin, G. L.; Mansfield, K.; Layman, J.; Sanders, E.; Simpson, D. G.; Wnek, G. E. *Polymer Preprints (American Chemical Society, Division of Polymer Chemistry)* **2002**, *43*, 457-458.

(29) Kenawy, E.-R.; Abdel-Fattah, Y. R. *Macromolecular Bioscience* **2002**, *2*, 261-266.

(30) Gibson, P.; Schreuder-Gibson, H.; Pentheny, C. *Journal of Coated Fabrics* **1998**, *28*, 63-72.

(31) Fridrikh, S. V.; Yu, J. H.; Brenner, M. P.; Rutledge, G. C. *Physical Review Letters* **2003**, *90*, 144502/144501-144502/144504.

(32) MacDiarmid, A. G.; Jones, W. E.; Norris, I. D.; Gao, J.; Johnson, A. T.; Pinto, N. J.; Hone, J.; Han, B.; Ko, F. K.; Okuzaki, H.; Llaguno, M. *Synthetic Metals* **2001**, *119*, 27-30.

(33) McKee, M. G.; Wilkes, G. L.; Colby, R. H.; Long, T. E. *Macromolecules* **2004**, *37*, 1760-1767.

(34) Demir, M. M.; Yilgor, I.; Yilgor, E.; Erman, B. *Polymer* **2002**, *43*, 3303-3309.

(35) Lee, K. H.; Kim, H. Y.; La, Y. M.; Lee, D. R.; Sung, N. H. *Journal of Polymer Science: Part B: polymer Physics* **2002**, *40*.

(36) Liu, H.; Hsieh, Y.-L. *Journal of Polymer Science, Part B: Polymer Physics* **2002**, *40*, 2119-2129.

(37) Morawetz, H. *High Polymers, Vol. 21: Macromolecules in Solution. 2nd Ed*, 1975.

(38) Hager, B. L.; Berry, G. C. *Journal of Polymer Science, Polymer Physics Edition* **1982**, *20*, 911-928.

(39) Flory, P. J. *Principles of Polymer Chemistry*, 1953.

(40) Tanford, C. *Physical Chemistry of Macromolecules*, 1961.

(41) Rai, P.; Rosen, S. L. *Journal of Polymer Science, Part B: Polymer Physics* **1997**, *35*, 1985-1987.

(42) Krause, W. E.; Bellomo, E. G.; Colby, R. H. *Biomacromolecules* **2001**, *2*, 65-69.

(43) Dobrynin, A. V.; Colby, R. H.; Rubinstein, M. *Macromolecules* **1995**, *28*, 1859-1871.

(44) De Gennes, P. G. *Macromolecules* **1976**, *9*, 594-598.

(45) De Gennes, P. G. *Scaling Concepts in Polymer Physics*, 1979.

(46) Adam, M.; Delsanti, M. *Journal de Physique (Paris)* **1982**, *43*, 549-557.

(47) Adam, M.; Delsanti, M. *Journal de Physique (Paris)* **1983**, *44*, 1185-1193.

(48) Takahashi, Y.; Isono, Y.; Noda, I.; Nagasawa, M. *Macromolecules* **1985**, *18*, 1002-1008.

(49) Pearson, D. S. *Rubber Chemistry and Technology* **1987**, *60*, 439-496.

(50) Colby, R. H.; Rubinstein, M. *Macromolecules* **1990**, *23*, 2753-2757.

(51) Colby, R. H.; Fetters, L. J.; Funk, W. G.; Graessley, W. W. *Macromolecules* **1991**, *24*, 3873-3882.

(52) Colby, R. H.; Rubinstein, M.; Daoud, M. *Journal de Physique II* **1994**, *4*, 1299-1310.

(53) Bordi, F.; Colby, R. H.; Cametti, C.; Lorenzo De, L.; Gili, T. *Journal of Physical Chemistry: Part B* **2002**, *106*, 6887-6893.

(54) Krause, W. E.; Tan, J. S.; Colby, R. H. *Journal of Polymer Science, Part B: Polymer Physics* **1999**, *37*, 3429-3437.

(55) Berne, B. J.; Pecora, R. *Dynamic Light Scattering: with Applications to Chemistry, Biology, and Physics*, 1975.

(56) Nagpal, V. J.; Davis, R. M.; Liu, Q.; Facinelli, J.; Riffle, J. S. *Langmuir* **1994**, *10*, 4434-4439.

(57) Dobkowski, Z. *Polimery (Warsaw, Poland)* **1984**, *29*, 238-239.

(58) Reneker, D. H.; Chun, I. *Nanotechnology* **1996**, *7*, 216-223.

(59) Yarin, A. L. *Free Liquid Jets and Films: Hydrodynamics and Rheology,*; Longman, Harlow and Wiley: NY, 1993.